Available online at www.sciencedirect.com
ScienceDirect
Journal of Colloid and Interface Science 312 (2007) 460–469
JOURNAL OF Colloid and Interface Science
www.elsevier.com/locate/jcis

Interfacial aspects of water drop formation at micro-engineered orifices

Maik J. Geerken, Rob G.H. Lammertink *, Matthias Wessling

Membrane Technology Group, Faculty of Science and Technology, University of Twente, P.O. Box 217, 7500 AE Enschede, The Netherlands

Received 22 February 2007; accepted 31 March 2007

Available online 7 April 2007

Abstract

The formation of emulsions with micro-engineered silicon based arrays of micro-orifices is a relatively new technique. Until now, only the preparation of oil-in-water emulsions was studied due to the hydrophilic nature of silicon. This work evaluates the emulsification of water into *n*-hexadecane with hydrophobized arrays of micro-orifices. We have studied the drop formation rate, the number of active pores and the drop size. In contrast to conventional macroporous membranes used for membrane emulsification, we observed high dispersed phase fluxes up to 4600 $L\,h^{-1}\,m^{-2}\,bar^{-1}$ while all pores being active at applied pressures below 2 times the critical pressure. The drop diameter was independent from the applied pressure difference. We observed a pressure dependent lag time between drop formations at low emulsification pressures. The lag time is related to the rate of surfactant diffusion to the water–oil interface causing a reduction of the interfacial tension. A significant influence of the used hydrophobization agents, perfluorinated octyltrichlorosilane (FOTS) and octyltrichlorosilane (OTS), was found for the resulting drop sizes and the number of active pores.

Keywords: Emulsification; Micro; Silicon; Interface

1. Introduction

Emulsification techniques are widely used in food, pharmacy, and cosmetic industry to produce oil-in-water or water-in-oil emulsions. Commonly used techniques include rotor–stator systems, high-pressure homogenizers, and ultrasound [1]. Due to high shear forces, the dispersed phase is divided into small droplets, stabilized by surfactants. However, shear stress and thermo sensitive ingredients, such as proteins, may loose their bioactivity during this process [2]. Muschiolik et al. [3] showed that whey proteins could change their physico-chemical properties due to a high pressure treatment. The whey protein β-lactoglobulin for instance looses its emulsifying efficiency due to pressure-induced unfolding resulting in protein aggregation [4].

Cross-flow membrane emulsification is a relative new emulsification process. This technique requires less energy, generates less stress to the ingredients and produces narrow drop size distributions [5]. In this process, the dispersed phase is forced through a porous membrane into the flowing continuous phase (see Fig. 1).

Lately, different types of membranes were employed for membrane emulsification having pore sizes in the micrometer range. As Table 1 indicates, most of them were exploited for

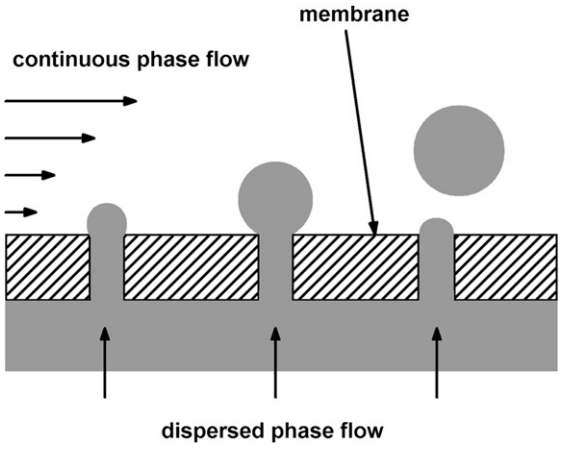

Fig. 1. Schematic drawing of the emulsification process with a porous membrane to produce water-in-oil emulsions.

* Corresponding author. Fax: +31 53 489 4611.
E-mail address: r.g.h.lammertink@utwente.nl (R.G.H. Lammertink).

0021-9797/$ – see front matter
doi:10.1016/j.jcis.2007.03.074

Table 1
Membranes used for cross-flow membrane emulsification

Membrane material	Type of emulsions	Ref.
Al_2O_3	Oil-in-water	[6,7]
Shirasu porous glass (SPG)	Oil-in-water	[8–10]
Polycarbonate (PC)	Oil-in-water	[11]
Polypropylene (PP)	Water-in-oil	[12]

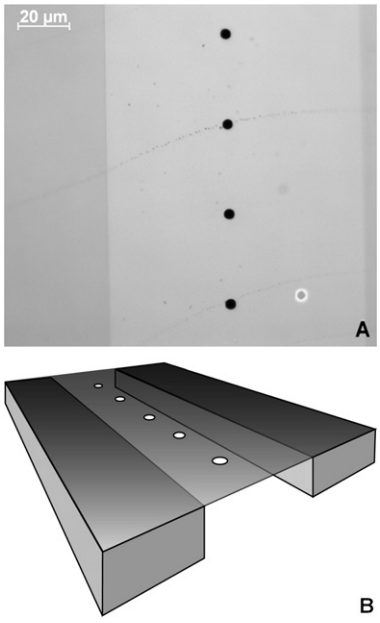

Fig. 2. Optical image of 3.5 µm micro-orifices (A) and a schematic representation of the micro-orifice array designed for emulsification application (B). Further details can be found in Section 2.

the production of oil-in-water emulsions requiring hydrophilic membranes.

Until now, membrane emulsification technology has not found its way to large-scale manufacturing, because commercially available membranes possess some disadvantages. They require a high-pressure drop and consist of a highly porous and irregular morphology on a microscopic scale [13]. To overcome these disadvantages, a micro-engineered membrane was adopted from microfiltration [14,15]. This microsieve membrane, fabricated out of silicon nitride with a silicon support, has a precisely defined pore size and a narrow pore size distribution, combined with a micron-sized membrane thickness. Furthermore, the porosity can be optimized for emulsification to limit coalescence of neighboring drops as displayed in Fig. 2.

It is frequently stated, that membrane emulsification needs a surface that is not wetted by the dispersed phase. To our knowledge, only the work of Kobayashi et al. [11] clearly shows for different emulsifiers that successful emulsification of oil into water only occurs if the oil phase does not wet the membrane surface. In our recent paper we proved that a hydrophobic surface is required for producing water-in-oil emulsion [16]. Due to the silicon nitride processing conditions, groups like silanol (SiOH), primary ($SiNH_2$), and secondary amino groups (Si_2NH) are present [17]. Overall, this results in a relatively hydrophilic surface with water/air contact angles of 65°.

To perform successful emulsification of water into an oil phase, the surface properties of silicon nitride have to be changed into a hydrophobic state. A possible way to achieve surface hydrophobicity is the deposition of self-assembled monolayers of alkyltrichlorosilanes. These kinds of monomolecular coatings are hydrophobic and they show a good thermal and chemical stability [18].

In this paper we discuss interfacial aspects of water drop formation at silicon nitride micro-orifices to produce water-in-oil emulsions. Until now, only oil-in-water emulsification with silicon nitride arrays of micro-orifices was investigated. Within these studies, it was found that only a few percentages of the nozzles were active and that the drops were not formed continuously at the single nozzles [13]. A physical reason for this period of inactivity was not given. Here, we will show that the nozzle activity reaches 100% at relatively low pressures and that the discontinuity of the drop formation is related to the dynamic interfacial tension of the used water–oil–surfactant system.

2. Experimental

2.1. Chemicals

n-Hexadecane (Merck) was used as the continuous phase containing either 1 wt% BolecMT (Loders Croklaan B.V.) or 1 wt% Span85 (sorbitan-trioleate; Merck). BolecMT is a soybean based industrial emulsifier containing approximately 40 wt% mono-, di-, and tri-glycerides, 36 wt% phospholipids, 18 wt% free fatty acids and 6 wt% proteins, polysaccharides and seed residues. For the dispersed phase MilliQ-water was used.

For the self-assembled monolayer formation two types of alkyltrichlorosilanes were used. Octyltrichlorosilane (OTS) (Aldrich, 97%) and perfluoro-octyltrichlorosilane (FOTS) (Fluka, >97%) were used as received.

2.2. Micro-nozzle plates

Two types of silicon nitride micro-orifice arrays received from Aquamarijn Micro Filtration B.V. were used. The first one had nozzles with 2.5 µm in diameter arranged in three single row nozzle fields with distances of 100 µm between the nozzles.

The second used micro-orifice array (see Fig. 2) had nozzles with a diameter of 3.5 µm arranged in one single row and two double row nozzle fields. The distance between the nozzles in all fields was 35 µm. The nozzle fields were separated by several hundreds of micrometer. The backsides of the nozzle fields for both arrays were fully open to guarantee a high accessibility for the dispersed phase without generating additional flow resistance. The thickness of the micro-orifice array within the nozzle fields was 1 µm.

2.3. Surface modification

As a pre-treatment, the micro-orifice arrays were cleaned and oxidized using a reactive oxygen plasma (Plasmafab 508, Electrotech; 10 min, 500 W, $pO_2 = 16$ mbar).

For the chemical vapor deposition of silane monolayers plasma oxidized silicon nitride micro-orifice arrays were stored together with a few microliters of FOTS or OTS in a dry and sealed glass box. The heat treatment was carried out at 120 °C for 2 h in a nitrogen flushed oven. Afterwards the micro-orifice arrays were allowed to cool down to room temperature while staying in the oven followed by a stabilization step at 100 °C for 1 h. The modification process was finished by extensively rinsing first with isopropanol, then with ultra pure water and dried with nitrogen. After these modifications surfaces coated with OTS and FOTS showed water contact angles of $104 \pm 2°$ and $114 \pm 1°$, respectively.

2.4. Interfacial tension and static contact angle

The dynamic interfacial tension measurements of BolecMT were conducted with a drop volume tensiometer (Lauda) at the University of Karlsruhe, Institut für Lebensmittelverfahrenstechnik (Germany). Static contact angles were measured with a goniometer (OCA 15, Data Physics).

2.5. Emulsification set-up

In order to visualize and quantify the drop formation process the micro-orifice arrays were placed into a module with a transparent cover slide designed for studying the filtration performance of silicon nitride microsieves shown in Figs. 3B and 3C [19]. The continuous (oil) and the dispersed phase (water) were fed into the module via gear pumps with maximum flow rates of 100 $\mathrm{L\,h^{-1}}$ for the continuous phase and 1 $\mathrm{L\,h^{-1}}$ for the dispersed phase (Verder Pumps). Both phases were recirculated within the system. To prevent blocking of the nozzles the dispersed phase (water) was pre-filtered inline with a 0.45 µm cellulose acetate filter (Schleicher & Schuell).

The dispersed phase pressure was adjusted either with a needle valve or by changing the dispersed phase flow rate and monitored via a pressure sensor (Keller AG) connected to a data acquisition system. The continuous phase pressure was measured next to the position of the micro-orifice array inside the module and collected as well by a data acquisition system. The data acquisition system was obtained from National Instruments equipped with two signal read-out cards and a serial interface connected to a personal computer. For the signal processing and for the calculation of the applied pressure difference ($\Delta p = p_{\text{dispersed phase}} - p_{\text{continuous phase}}$) a Labview program was used. The entire set-up is shown schematically in Fig. 3A.

The visualization was performed using an inverted optical microscope (Zeiss Axiovert) equipped with a CCD camera providing a maximum frame rate of 8 frames per second. Although slow, this rate is sufficiently accurate to observe the drop formation process at low emulsification pressures and low cross-flow velocities.

The set-up was cleaned first with an aqueous detergent solution (Lux, Unilever, contains anionic and amphoteric surfactants) followed by a 1–2 vol% aqueous Deconex solution (Borer Chemie; contains KOH). Both cleaning steps were performed

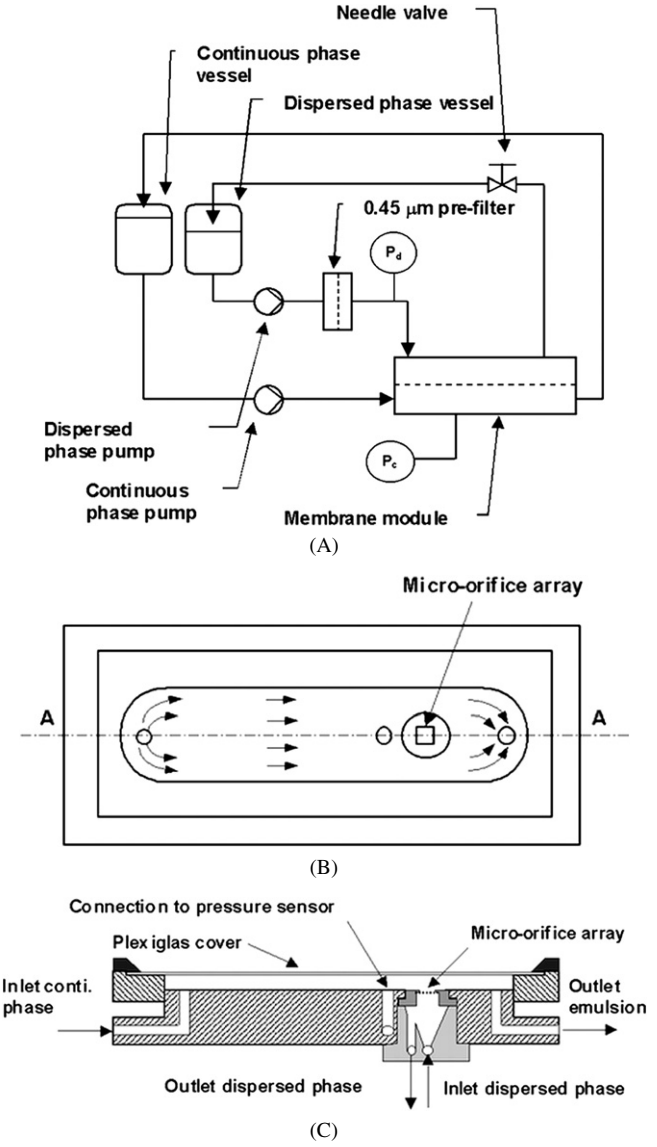

Fig. 3. Cross-flow membrane emulsification set-up (A), top view (B) and cross-section (C) of the emulsification module.

at room temperature and low pressure. Afterwards the set-up was rinsed several times with ultra pure water. Before drying with air the ultra pure water was pressed out with air followed by flushing isopropanol through the system. After each experiment, the oil phase was pressed out with air before starting the mentioned cleaning procedure.

Used micro-orifice arrays were cleaned separately from set-up and were replaced inside the set-up with a dummy array. The micro-orifice arrays were first washed with the aqueous detergent solution, then rinsed with tap water and followed by MilliQ-water, and finally with isopropanol. All rinsing and washing steps were performed at room temperature. Afterwards, the micro-orifices arrays were dried first in a nitrogen stream and then at 80 °C.

The hydrophobized micro-orifice arrays were fixed and sealed within stainless steel holders with silicon glue (TSE 399C, GE Bayer Silicons). To start an experiment, the holder including a micro-orifice array was mounted into the emulsi-

fication module and connected to the dispersed phase supply tubing. Then both liquid phases were slowly pumped into the system at low pressure. At the same time the pressure data acquisition system was started. After the set-up was completely filled with both phases, the desired continuous phase velocity of 0.074 $m\,s^{-1}$ was adjusted. Higher velocities were not explored due to the restrictions of the CCD camera. However, increasing the cross-flow velocity leads to smaller drop sizes as already reported in several studies [2,5,7,11]. The dispersed phase pressure was step-wise increased until first droplet formation occurred. From there on the dispersed phase pressure was adjusted. At each pressure step two movies of minimum 30 s were recorded.

Individual frames were extracted from the movies with a video converter program and the drop size, the drop formation rate and the number of active nozzles were achieved from single frames with the imaging software Scion Image® (Scion Corporation).

3. Results and discussion

3.1. Drop formation rate

The drop formation process starts when the pressure difference exceeds the critical pressure (p_{critical}), which is determined by the pore radius (r_{Nozzle}) and the interfacial tension (γ) according to equation

$$p_{\text{critical}} = \frac{2\gamma}{r_{\text{Nozzle}}}. \tag{1}$$

For the 2.5 μm array and 1 wt% BolecMT the experimentally obtained critical pressure is equal to 183 mbar and for the 3.5 μm array and 1 wt% Span85 the value is 54 mbar as it can be seen in Fig. 4, which shows the drop formation rate versus the applied pressure difference.

The drop formation rate also accounts for the increasing number of active pores with increasing pressure. When doing this, we found a linear relationship with the intercept at the x-axis giving the critical pressure of the used surfactant containing system. These pressures correspond to interfacial tensions of 11.4 for BolecMT and 4.7 $mN\,m^{-1}$ for Span85, respectively. The slope of the regression lines in Figs. 4A and 4B corresponds to the resistance of the nozzles following Darcy's law. To obtain the flow resistance of the nozzles, the average dispersed phase flow through the nozzles ($\dot{V}_{\text{dispersed phase}}$) is calculated by dividing the average drop volume with the average drop inflation time. The actual flow resistance is calculated via

$$R_{\text{Nozzle}} = \frac{(\Delta p - p_{\text{critical}})}{\dot{V}_{\text{dispersed phase}}\,\eta_{\text{dispersed phase}}} \tag{2}$$

and the theoretical flow resistance according to

$$R_{\text{Nozzle,HP}} = \frac{128 l_{\text{Nozzle}}}{\pi d_{\text{Nozzle}}^4}. \tag{3}$$

Equation (3) might not be applicable for volumetric flow through nozzles with small length/diameter ratio. In this case

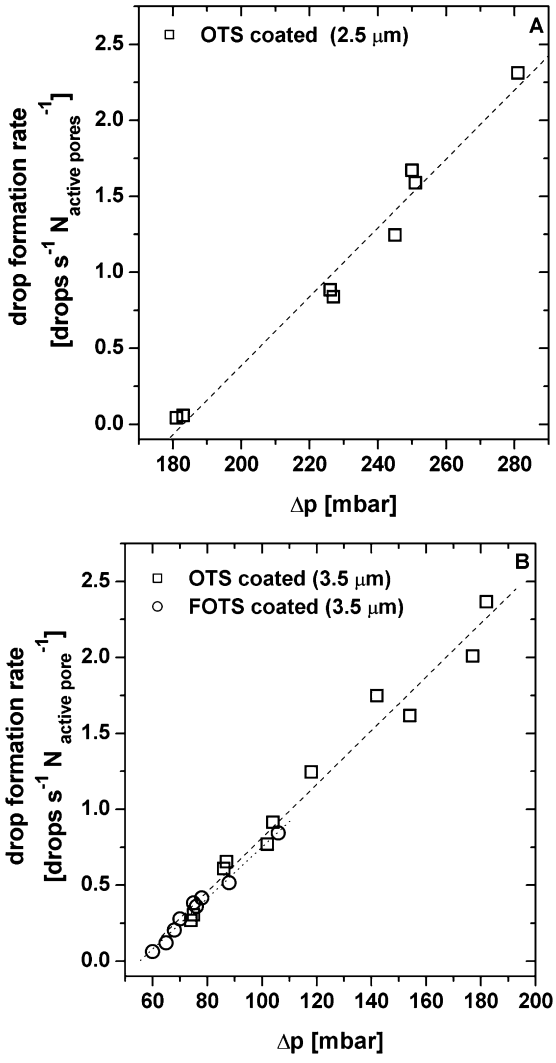

Fig. 4. Drop formation rate versus applied pressure difference (Δp) of water drops emulsified (A) into 1 wt% BolecMT containing n-hexadecane with a 2.5 μm micro-orifices array and (B) into 1 wt% Span85 containing n-hexadecane with a 3.5 μm micro-orifices array.

the total resistance is approximately the sum of Hagen–Poiseuille's resistance (Eq. (3)) and Sampson's resistance leading to equation [20,21]

$$R_{\text{Nozzle,HP+S}} = \frac{128 l_{\text{Nozzle}}}{\pi d_{\text{Nozzle}}^4} + \frac{24}{d_{\text{Nozzle}}^3}. \tag{4}$$

From Eq. (2) the flow resistance for the 2.5 μm nozzle is $(3.64 \pm 1.1) \times 10^{18}\ m^{-3}$ which is in the same order of magnitude compared to the theoretical resistance ($R_{\text{Nozzle,HP}} = 1.04 \times 10^{18}\ m^{-3}$) according to Eq. (3). Considering the small length/diameter ratio the theoretical flow resistance (Eq. (4)) is $2.58 \times 10^{18}\ m^{-3}$ and agrees even more with the experimental value. The experimental flow resistances (Eq. (2)) obtained from the 3.5 μm nozzle arrays coated with FOTS and OTS are $(1.56 \pm 0.41) \times 10^{17}\ m^{-3}$ and $(1.23 \pm 0.6) \times 10^{17}\ m^{-3}$, respectively. These values are as well in same order of magnitude compared to the theoretical values ($R_{\text{Nozzle,HP}} = 2.72 \times 10^{17}\ m^{-3}$ and $R_{\text{Nozzle,HP+S}} = 8.31 \times 10^{17}\ m^{-3}$). The derivations between the found experimental flow resistances and the

Table 2
Dispersed phase flux obtained here in comparison with different membranes found in literature

Type of membrane	Mean pore size (μm)	Δp (bar)	Dispersed phase	Flux ($L\,h^{-1}\,m^{-2}\,bar^{-1}$)	Ref.
Si_xN_y micro-orifices[a]	3.5	0.177	Water	4600	Present work
Si_xN_y micro-orifices	7	0.09	*n*-Hexadecane	21000	[13]
Silicon MC	17.3	0.108	Soybean oil	600	[25]
SPG membrane	2.5	0.264	Rape seed oil	11	[10]
Ceramic membrane	0.2	1.4	Mineral oil	14	[22]
PP hollow fiber	0.4	0.76	Water	0.26	[12]
MPG membrane	0.5	3.5	Sunflower oil	13	[23]

[a] Hydrophobized with OTS.

Table 3
Number of active pores and membrane properties

	D_{pore} (μm)	Thickness (μm)	Porosity (%)	No. of active pores (%)	At *x* times $P_{critical}$	Ref.
SPG-membrane	15	1000	53	0.5	6	[24]
Silicon microchannel	17.3	200	1.2	95	10	[25]
Si_xN_y microsieve	7	1	0.12	16	3	[13]
Micro-orifice array[a]	3.5	1	0.25	100	1.6	Present work
Micro-orifice array[b]	2.5	1	0.05	100	1.3	Present work

[a] Hydrophobized with FOTS.
[b] Hydrophobized with OTS.

theoretical values can arise from the variations of the drop volume and the drop formation times, which are in range of 5–25% for the drop volume and up to 50% for the drop formation time. Both are resulting at first from the low time resolution of the CCD camera and at second from the less controlled drop formation process at high drop formation rates and nozzle activities.

The dispersed phase flux in our experiments was remarkable high compared to conventional macroporous membranes and comparable to the flux obtained for oil-in-water emulsification with silicon nitride micro-orifice arrays as indicated in Table 2. The flux value was calculated from the average drop volume ($\overline{V}_{Drop}$), the drop formation rate and the number of active nozzles ($N_{active\,Nozzles}$) according to

$$\text{Flux} = \frac{\overline{V}_{Drop} \cdot \text{Drop formation rate} \cdot N_{active\,Nozzles}}{\Delta p \cdot A_{Array}}. \quad (5)$$

The considered array area (A_{Array}) was 1.599×10^{-7} m^2 and represents only the observed unsupported area of the micro-orifices array.

The most distinguishing feature between conventional membranes and the silicon based micro-orifices arrays is their thickness and morphology. The conventional membranes have a thickness ranging from 50 to several hundreds of micrometer. The morphology is tortuous and pore sizes are polydisperse. Thickness and tortuosity will lead to a high membrane resistance.

The pure water flux for polypropylene hollow fibers was measured to be 6000 times higher than the water flux in a membrane emulsification experiment [12]. Contrary to the high porosity of the conventional membranes, which enables a high pure liquid permeability, Vladisavljevic and Schubert [10] calculated that for SPG membranes only 2% of the pores were active within emulsifying oil into water. The interfacial tension between oil and water influences the permeability of the dispersed phase in highly porous and tortuous membranes to a great extend.

The silicon based micro-orifices arrays are extremely thin and have an optimized morphology. The porosity is quite low to prevent coalescences of growing drops. Here, in contrast to Vladisavljevic et al. the percentage of active pores was extremely high. The percentage of active nozzles was over 90% in case of the 2.5 μm array in combination with BolecMT, reached at 1.25 times the critical pressure. For the 3.5 μm micro-orifices array coated with OTS the percentage of active nozzles was about 60% at 3.3 times the critical pressure. For the same arrays coated with FOTS the nozzle activity reached 100% at 1.6 times the critical pressure. For comparison, these values are listed in Table 3.

Only a few papers have reported the number of active pores (nozzles) obtained by visualization of the drop formation process. The optical observation of the oil drop formation into a 0.3 wt% SDS aqueous solution using a 10 μm hydrophilic polycarbonate track-etch membrane showed only 1 percent of active pores just above the critical pressure of 13.5 mbar. Unfortunately, no data is given for higher pressures [11]. A SPG membrane with a mean pore size of 15 μm used to emulsify soybean oil into 0.3 wt% SDS aqueous solution showed an increase of the number of active pores from 0.3 to 0.5% while the dispersed phase flux was increased by a factor of six [24]. For rectangular straight-through microchannels with a hydraulic diameter of 17.3 μm, the number of active microchannels increased from 10 to 95% with the increasing pressure from 1.8 mbar (critical pressure) to 18 mbar. As dispersed phase soybean oil was used and emulsified into a 0.3 wt% SDS aqueous solution [25]. Abrahamse et al. [13] reported at 3 times the critical pressure for a 7 μm silicon nitride micro-orifice array that 16% of the pores

were active during the emulsification of hexadecane into 1 wt% Tween20 aqueous solution. The reason for the low pore activity was explained by the small ratio of the pore resistance (R_p) over the substructure resistance (R_s) against flow. The ratio found for the 7 μm silicon nitride array was 3.7. The authors claim that a higher ratio leads to a higher number of active pores [26]. Here, micro-orifice arrays were used with an open substructure, which results in a lower flow resistance in the substructure, and with smaller pore sizes resulting in higher flow resistances in the pores. This increases the ratio of R_p over R_s compared to Gijsbertsen-Abrahamse et al. [26] by a factor of 14 and explains the differences between the high percentage of active pores reported in our work and low activity reported by Abrahamse et al. [13]. Table 3 suggests also that the surface porosity influences the number of active pores.

3.2. Drop size

The formed water drops had diameters in the range of 100–200 μm as shown in Fig. 5. They were one order of magnitude larger than the nozzle diameter of the used arrays. In order to observe the drop formation process we performed the emulsification at low cross-flow velocities resulting in relative large drops. The drop to nozzle diameter ratio was 45 and 52 for the 2.5 μm arrays coated with OTS and FOTS. For the 3.5 μm arrays the ratio was 40 for the OTS coated one and 52 for the FOTS coated array.

The coefficient of variation, which is the standard deviation divided by the average drop size, varied between 5 and 25% and increased with increasing number of active pores. At high pore activity growing and detaching drops were interfering with drops growing next to it. This results in a less controlled drop detachment of neighboring drops and larger drop size variations. As already indicated before, the drops produced with FOTS coated arrays were for both pore sizes and both surfactants larger compared to those produced via OTS coated arrays. This is related to the approximately 20° lower contact angle of water in surfactant containing hexadecane on FOTS coated substrates [16].

The drop diameter was independent of the applied pressure for both observed emulsifier systems and for both hydrophobic coatings as depicted in Fig. 5. Van der Graaf et al. [27] reported that the drop size increases at constant emulsifier concentration if the applied pressure difference increases. These observations can be related to the adsorption rate of the emulsifier on a growing droplet. Schröder and Schubert [2] suggested that the influence of the dispersed phase pressure becomes less as the emulsifier adsorbs faster. When the fast emulsifier SDS is used, the drop diameter is nearly independent from the applied dispersed phase pressure [2,24].

The dynamic interfacial tension is a major factor determining the final drop size. It forces the drop to remain attached to the pore as long as the interfacial tension force is higher than the shear force applied by the cross-flowing continuous phase (Fig. 6). When the pressure is increased, the drop grows faster while the adsorption kinetic of the emulsifiers is not changed. The higher interfacial tension force keeps the drop attached to

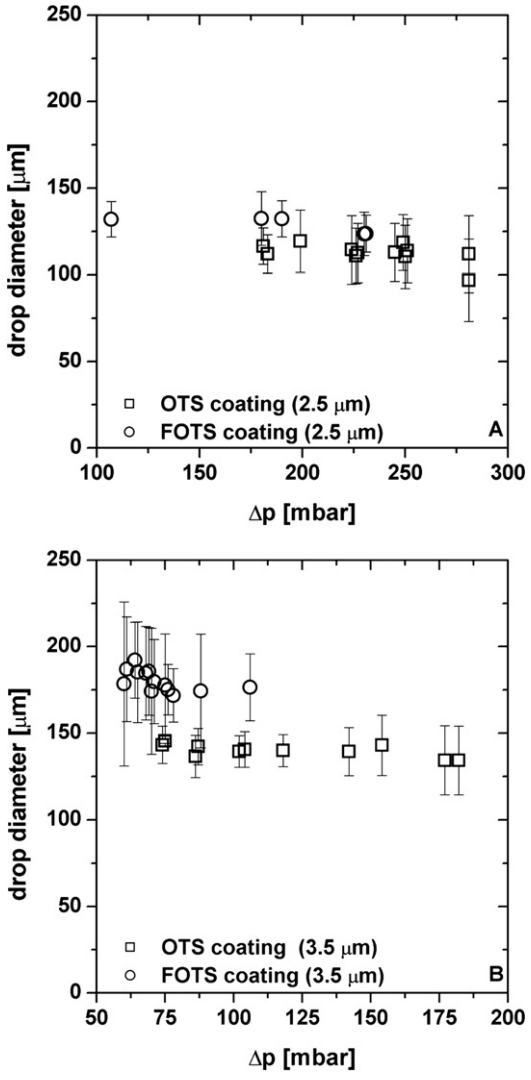

Fig. 5. Average drop diameter versus applied pressure difference (Δp) of water drops emulsified (A) into 1 wt% BolecMT containing n-hexadecane with 2.5 μm OTS and FOTS coated arrays and (B) into 1 wt% Span85 containing n-hexadecane with 3.5 μm OTS and FOTS coated arrays.

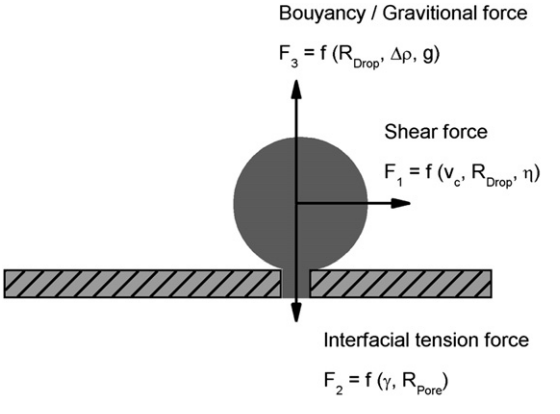

Force balance:

$$6\,\pi\, v_{\text{conti. ph.}}\, R_{\text{Drop}}\, \eta_{\text{conti. ph.}} + 4/3\,\pi\, R^3_{\text{Drop}}\, \Delta\rho\, g = 2\,\pi\,\gamma\, R_{\text{Pore}}$$

Fig. 6. Schematic drawing of the major forces acting on a droplet inflated from a pore into the parallel to a membrane flowing continuous phase.

the pore. At constant cross-flow velocity the shear force scales with the drop diameter. Hence, the drop grows until a diameter is reached at which the shear force is higher than the interfacial tension force. For fast adsorbing emulsifiers the interfacial tension will be close to its equilibrium value. In our case, however, BolecMT is used, which is a very slow adsorbing emulsifier [16]. This suggests that another regime exist where the drop diameter is independent from the applied pressure. In the first regime the adsorption of the emulsifier is fast enough to compensate the surfactant dilution of the interface caused by the expansion of the growing drop. Therefore, the final interfacial tension is not significantly changing over a certain pressure range. While in the other regime, after the initial adsorption to start drop growth, the surfactant adsorption rate is far lower than the surfactant surface dilution rate. Therefore, the interfacial tension increases due to surfactant dilution at the interface caused by its growth and insufficient replenishment out of the continuous phase.

3.3. Lag time

During the visual observation of the drop formation it was found that the drops were not formed continuously at low pressure differences. After detachment of a drop the pore remained inactive for a certain period of time before a new drop was inflated as depicted in Fig. 7. The period of inactivity is called lag time and was firstly reported by Abrahamse et al. [13]. Van der Graaf et al. [27] did not observe any lag time. Today, no physical reason for the lag time nor the conditions at which a lag time occurs are reported. Here, we will prove that the lag time is a subtle measure for the dynamic interfacial tension of the oil–water–surfactant system.

A lag time was found for all observed pores during all performed experiments. The most obvious finding concerning the lag time was the decrease of the lag time with increasing pressure difference. Fig. 8 shows the pressure difference plotted as a function of the inverse square root of the lag time. For 1 wt% Span85 we observe a clear linear relationship (Fig. 8B). For 1 wt% BolecMT (Fig. 8A) the linear relation holds only for pressure differences above 180 mbar. We will explain this observation later in this section. Based on the data reported by Abrahamse et al. [13] we calculated the lag time for the hexadecane–water–Tween20 system used in their study. The applied pressure difference showed as well a linear function of the inverse square root of the lag time.

The relation between the lag time and the pressure difference can be explained with the critical Laplace pressure. This pressure has to be overcome by the applied pressure difference to inflate a drop from a nozzle and corresponds to the Laplace pressure of a hemispherical interface at the nozzle opening. The second variable to take into account is the interfacial tension (IFT). For a certain Δp and a given nozzle diameter the IFT has to reach a value which corresponds to the critical Laplace pressure. As long as the applied pressure difference is lower compared to the Laplace pressure drop formation will not occur.

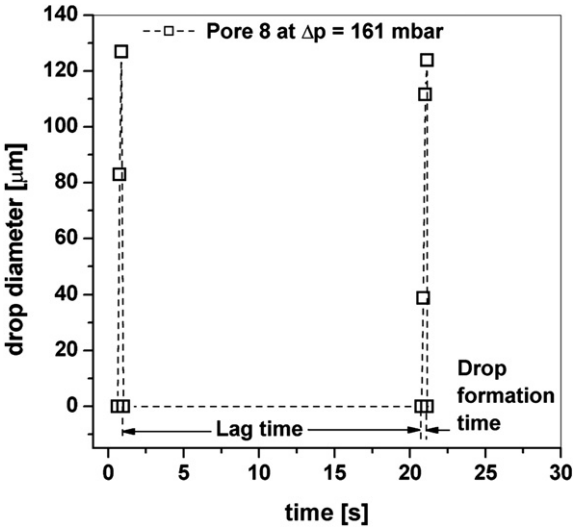

Fig. 7. Growth of water drops from a single pore at 161 mbar (2.5 μm OTS coated array; 1 wt% BolecMT dissolved in *n*-hexadecane).

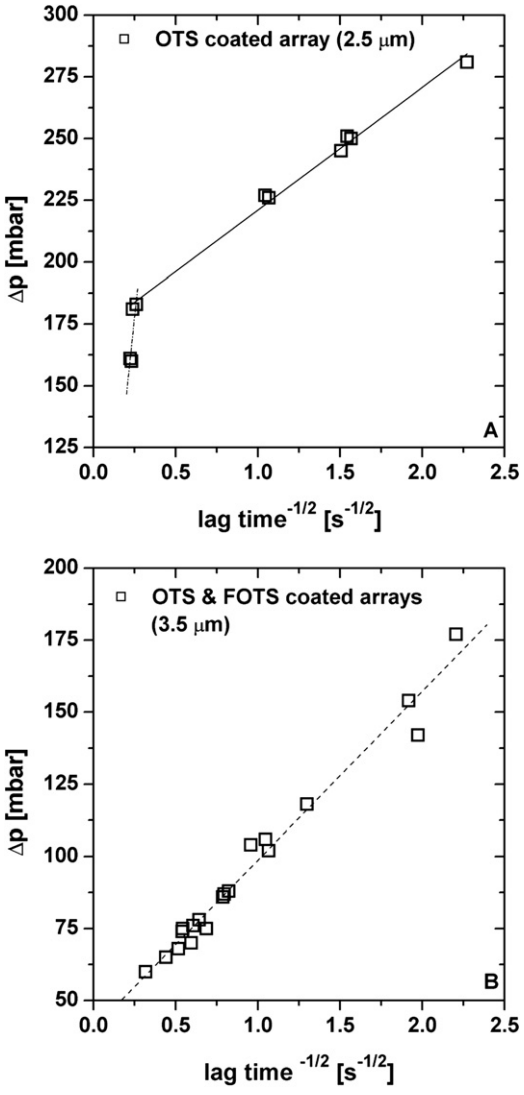

Fig. 8. Applied pressure difference (Δp) versus the inverse square root of lag time for (A) 1 wt% BolecMT and (B) 1 wt% Span 85.

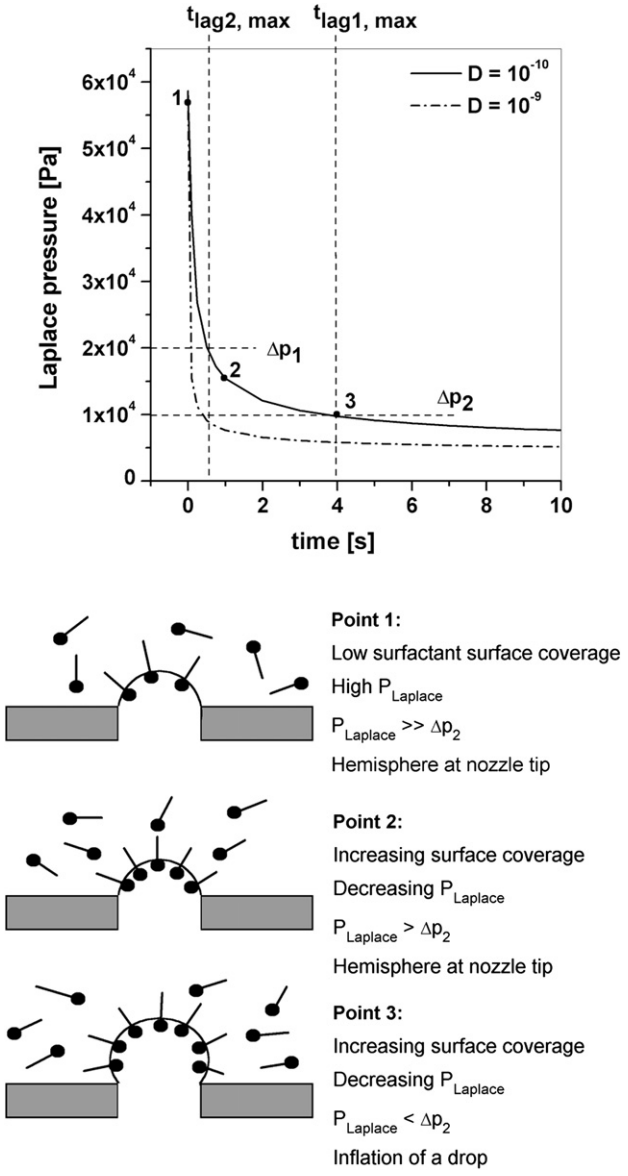

Fig. 9. Decline of the Laplace pressure with adsorption time. Calculated via Eqs. (1) and (6) for a nozzle size of 3.5 μm and two different diffusion coefficients.

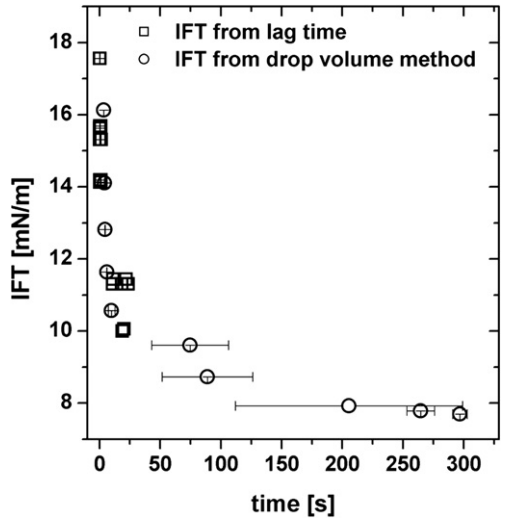

Fig. 10. Comparison between interfacial tension of water/*n*-hexadecane +1 wt% BolecMT obtained from lag time at a 2.5 μm orifice and from drop volume method.

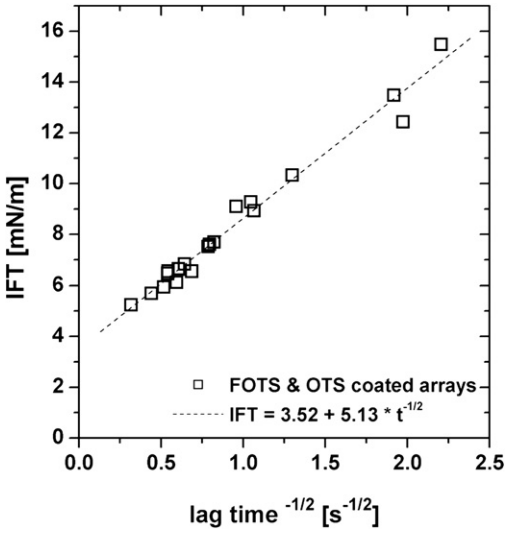

Fig. 11. Interfacial tension (calculated via Eq. (1)) versus the negative square root of the lag time plotted according to Eq. (6) of 1 wt% Span85.

After drop detachment, a sufficient amount of surfactants have to adsorb at the hemispherical interface before the critical Laplace pressure is reached again. The adsorption of surfactants at an interface is a kinetic process and is represented by the dynamic interfacial tension of a given surfactant.

Fig. 9 illustrates qualitatively the relation between the lag time and the pressure difference. The dynamic interfacial tension is derivate from Eq. (6) and translated into pressure with Eq. (1). If the emulsification process operates at low pressure difference (Δp_2 in Fig. 9) then the Laplace pressure has to decrease by the surfactant adsorption to a relatively low value (from point 1 to point 3). The absolute value of the lag time depends on the corresponding interfacial tension at the moment of drop detachment (point 1). For faster adsorbing surfactants, indicated by a higher diffusion coefficient, the lag time reduces, because the required critical interfacial tension is reached at earlier (lag) times. Following the same arguments explains that increasing the pressure difference leads to a decreasing lag time.

We can conclude that the lag time appears to be a sensitive measure of the dynamic interfacial tension. To prove this, for each applied pressure difference the corresponding interfacial tensions were calculated according to the Laplace pressure equation (Eq. (1)), plotted against the observed lag times and in case of 1 wt% BolecMT compared with the dynamic interfacial tension obtained by the drop volume method. The results are plotted in Fig. 10. The dynamic interfacial tension derived from the lag time fits well to the values from the drop volume method.

Recalling the inverse square root relation between the lag time and Δp, Fig. 11 depicts the same for the IFT of 1 wt% Span85. This type of plot is typical for presenting the dynamic interfacial tension of a given emulsifier containing system. Ba-

sis for these plots is the so-called long time approximation for the dynamic interfacial tension [28].

$$\gamma(t) - \gamma_{eq} = \frac{RT\Gamma_c^2}{C_0}\sqrt{\frac{\pi}{4Dt}}. \quad (6)$$

Equation (6) is a simplified version of the equation of Ward and Tordai relating the interfacial tension decline with the surfactant bulk concentration C_0, the adsorbed emulsifier density Γ_c and the diffusion coefficient D. From the intercept of the linear regression line in Fig. 11 the equilibrium interfacial tension of 3.5 ± 0.2 mN m^{-1} is obtained. This value agrees with the equilibrium interfacial of 3.3 ± 0.1 mN m^{-1} for 1 wt% Span85 obtained from sessile drop measurements.

The interfacial tension of 1 wt% BolecMT does not follow the linearity of Eq. (6) over the entire time range. Only at short adsorption times the values agree with it. This emulsifier is a mixture of phospholipids and proteins and its adsorption on interfaces is a competitive process. Therefore, its interfacial tension decline differs from single component adsorption as we showed in an earlier work [16].

As indicated by Eq. (6) the slope and the intercept of the regression line in Fig. 11 can be influenced by varying the surfactant concentration and by using surfactants with different diffusion coefficients. Considering the first, concentrations below the critical micelle concentration (CMC) will result in a steeper slope and a higher intercept. For concentrations above the CMC almost no change is expected. Secondly, for emulsifiers with higher diffusion coefficients the slope will increase. In conclusion, the lag time will be shorter or disappears at a given pressure difference for higher surfactant concentrations and for surfactants with higher diffusion coefficients.

In general, a lag time appears in an emulsification process at pressures close to the critical pressure and in combination with slow or medium fast adsorbing emulsifiers. It disappears if the applied pressure is increased or faster adsorbing emulsifiers are used.

4. Conclusions

We could demonstrate successful emulsification of water into *n*-hexadecane with hydrophobic arrays of micro-orifices. Significant differences between FOTS and OTS coatings were found for the drop diameter caused by different contact angles with in the system of water/*n*-hexadecane + surfactant/coated substrate. The different hydrophobic coatings do not significantly influence the drop formation rate, the percentage of active pores and the lag time. The extremely low porosity and the open back structure of the used micro-orifice arrays result in nearly 100% active pores at less than two times the critical pressure.

The observed lag time disappears at a certain Δp. For fast adsorbing emulsifiers like SDS a lag time is not observed. Therefore, two ways are possible to avoid the lag time. Using faster adsorbing emulsifiers or if this is not possible, due to restrictions of the usable emulsifiers within the product recipe, the applied pressure difference over the nozzles can be increased until the lag time vanishes.

Acknowledgments

The work was sponsored by the European Union (Thames Project; QLRT 2000-01228). Microsieve membranes were kindly provided by Aquamarijn B.V. The drop volume dynamic interfacial tension measurements were conducted by Uwe Lambrich from the University of Karlsruhe, Germany.

Appendix A. Nomenclature

CMC	critical micelle concentration
FOTS	perfluorinated octyltrichlorosilane
IFT	interfacial tension
MC	micro channel
MPG	micro porous glass
OTS	octyltrichlorosilane
PC	polycarbonate
PP	polypropylene
SDS	sodium dodecylsulfate
SPG	Shirasu porous glass
A_{array}	unsupported micro-orifice array area (m^2)
C_0	bulk emulsifier concentration (mol L^{-1})
D	emulsifier diffusion coefficient (m^2 s^{-1})
d_{Nozzle}	nozzle diameter (m)
l_{Nozzle}	length of a nozzle (m)
$N_{active\ Nozzle}$	number of actives nozzles (–)
Δp	applied pressure difference (bar)
$p_{continuous\ phase}$	pressure of the continuous phase (bar)
$p_{dispersed\ phase}$	pressure of the dispersed phase (bar)
$p_{critical}$	critical Laplace pressure (bar)
r_{Nozzle}	nozzle radius (m)
R	relative gas constant 8.314 (J K^{-1} mol^{-1})
R_{Nozzle}	experimental flow resistance of a nozzle (m^{-3})
$R_{Nozzle,HP}$	flow resistance of a nozzle according to Hagen–Poiseuille (m^{-3})
$R_{Nozzle,HP+S}$	sum of the Hagen–Poiseuille and Sampson flow resistance of a nozzle (m^{-3})
R_p	hydraulic pore resistance (m^{-3})
R_s	hydraulic substructure resistance (m^{-3})
T	temperature (K)
t	time (s)
$\overline{V}_{Drop}$	average drop volume (m^3)
$\dot{V}_{dispersed\ phase}$	average dispersed phase flow through a nozzle (m^3 s^{-1})

Greek letters

γ	interfacial tension (N m^{-1})
$\gamma(t)$	dynamic interfacial tension (N m^{-1})
γ_{eq}	equilibrium interfacial tension (N m^{-1})
Γ_c	emulsifier adsorption density (mol m^{-2})
$\eta_{dispersed\ phase}$	viscosity of the dispersed phase (Pa s)

References

[1] S. Sjöblom (Ed.), Encyclopedic Handbook of Emulsion Technology, Marcel Dekker, New York, 2001.

[2] V. Schröder, H. Schubert, Colloids Surf. A 152 (1999) 103.
[3] G. Muschiolik, S. Dräger, I. Scherze, H.M. Rawel, M. Stang, in: E. Dickinson, B. Bergeståhl (Eds.), Food Colloids, No. 192, The Royal Soc. Chem., Cambridge, 1997, p. 393.
[4] V.B. Galazka, E. Dickinson, D.A. Ledward, Food Hydrocolloids 10 (1996) 213.
[5] S.M. Joscelyne, G. Trägårdh, J. Membr. Sci. 169 (2000) 107.
[6] V. Schröder, O. Behrend, H. Schubert, J. Colloid Interface Sci. 202 (1998) 334.
[7] S.M. Joscelyne, G. Trägårdh, J. Food Eng. 39 (1999) 59.
[8] K. Kandori, in: A.G. Ganokar (Ed.), Food Processing: Recent Developments, Elsevier Science, Amsterdam, 1995, chap. 7.
[9] N.C. Christov, D.N. Ganchev, N.D. Vassileva, N.D. Denkov, K.D. Danov, P.A. Kralchevsky, Colloids Surf. A 209 (2002) 83.
[10] G.T. Vladisavljevic, H. Schubert, Desalination 144 (2002) 167.
[11] I. Kobayashi, M. Yasuno, S. Iwamoto, A. Shono, K. Satoh, M. Nakajima, Colloids Surf. A 207 (2002) 185.
[12] G.T. Vladisavljevic, S. Tesch, H. Schubert, Chem. Eng. Process. 41 (2002) 231.
[13] A.J. Abrahamse, R. van Lierop, R.G.M. van der Sman, A. van der Padt, R.M. Boom, J. Membr. Sci. 204 (2002) 125.
[14] C.J.M. van Rijn, M.C. Elwenspoek, IEEE Proc. MEMS (1995) 83.
[15] C.J.M. van Rijn, Nano and Micro Engineered Membrane Technology, Elsevier, Amsterdam, 2004, chap. 11.
[16] M.J. Geerken, R.G.H. Lammertink, M. Wessling, Colloids Surf. A 292 (2007) 224.
[17] B.V. Zhmud, J. Sonnefeld, L. Bergström, Colloids Surf. A 158 (1999) 327.
[18] M.J. Geerken, T.S. van Zanten, R.G.H. Lammertink, Z. Borneman, W. Nijdam, C.J.M. van Rijn, M. Wessling, Adv. Eng. Mater. 6 (2004) 749.
[19] M. Grionès, Z. Borneman, R.G.H. Lammertink, M. Wessling, J. Membr. Sci. 259 (2005) 55.
[20] J.M. Yang, C.-M. Ho, X. Yang, Y.-C. Tai, J. Fluids Eng. 123 (2001) 899.
[21] C.Y. Wang, Acta Mech. 148 (2001) 55.
[22] R.A. Williams, S.J. Peng, D.A. Wheeler, N.C. Morley, D. Taylor, M. Walley, D.W. Houldsworth, Trans. IChem E 76 Part A (1998) 902.
[23] I. Scherze, K. Marzilger, G. Muschiolik, Colloids Surf. B 12 (1999) 213.
[24] M. Yasuno, M. Nakajima, S. Iwamoto, T. Maruyama, S. Sugiura, I. Kobayashi, A. Shono, K. Satoh, J. Membr. Sci. 210 (2002) 29.
[25] I. Kobayashi, M. Nakajima, K. Chun, Y. Kikuchi, H. Fujita, AIChE J. 48 (2002) 1639.
[26] A.J. Gijsbertsen-Abrahamse, A. van der Padt, R.M. Boom, J. Membr. Sci. 217 (2003) 141.
[27] S. van der Graaf, C.G.P.H. Schroën, R.G.M. van der Sman, R.M. Boom, J. Colloid Interface Sci. 277 (2004) 456.
[28] B.B. Niraula, T.K. Chun, H. Othman, M. Misran, Colloids Surf. A 248 (2004) 157.